RESEARCH ARTICLE

Lignin-derived dual-function red light carbon dots for hypochlorite detection and anti-counterfeiting

Yixuan Chang[1,2,3], **Fanwei Kong**[1,2,3], **Zihao Zhu**[1,2,3], **Ziai Wang**[1,2,3], **Chunxia Chen**[1,2,3],
Xiaobai Li (✉)[1,2,3], **Hongwei Ma** (✉)[1,2,3]

1 Key Laboratory of Forest Plant Ecology, Ministry of Education, Engineering Research Center of Forest Bio-Preparation, College of Chemistry, Chemical Engineering and Resource Utilization, Northeast Forestry University, Harbin 150040, China
2 State Engineering Laboratory of Bio-Resource Eco-Utilization, Northeast Forestry University, Harbin 150040, China
3 Collaborative Innovation Center for Development and Utilization of Forest Resources, Harbin 150040, China

Abstract The efficient utilization of natural lignin, which is the main by-product of the cellulose industry, is crucial for enhancing its economic value, alleviating the environmental burden, and improving ecological security. By taking advantage of the large sp^2 hybrid domain of lignin and introducing amino functional groups, new lignin-derived carbon dots (SPN-CDs) with red fluorescence were successfully synthesized. Compared with green and blue fluorescent materials, red SPN-CDs have desirable anti-interference properties of short-wave background and exhibit superior luminescence stability. The SPN-CDs obtained exhibited sensitive and distinctive visible color with fluorescence-dual responses toward hypochlorite. Considering this feature, a portable, low-cost, and sensitive fluorescence sensing paper with a low limit of detection of 0.249 μmol·L^{-1} was fabricated using the SPN-CDs for hypochlorite detection. Furthermore, a new type of visible-light and fluorescence dual-channel information encryption platform was constructed. Low-concentration hypochlorite can be employed as an accessible and efficient information encryption/decryption stimulus, as well as an information "eraser", facilitating a safe and diversified transmission and convenient decryption of information. This work opens new avenues for high-value-added applications of lignin-based fluorescent materials.

1 Introduction

The advancement of stimuli-responsive fluorescent

E-mails: lixiaobai2008@126.com (Li X.), mahw@nefu.edu.cn (Ma H.)

materials with sensitive and specific optical responsiveness enables the development of various important technologies, including chemical sensors, optical switches, biological imaging, medical diagnosis, information storage, and anti-counterfeiting [1–6]. In recent decades, various fluorescent materials have been investigated, such as stimuli-responsive aggregation-induced emission molecules [7], metal−organic frameworks [8], and conjugated microporous polymers [9]. However, toxic raw materials and fluorescent products, as well as complex, costly, and environmentally unfriendly fabrication processes, restrict their widespread application. Therefore, the recent development of green and sustainable fluorescent materials has attracted significant interest.

Carbon dots, a new type of luminescent nanomaterial, have attracted considerable attention because of their small size, excellent optical properties, good water solubility, facile synthesis, and ease of surface modification [10]. More importantly, biomass-based carbon dots exhibit lower cytotoxicity and good biocompatibility, with excellent applications in various fields, such as ion detection [11], bioimaging [12], drug delivery [13], and photocatalysis [14].

Generally, hypochlorite (ClO$^-$) plays an important role in our daily life. It is a common domestic water disinfectant and dye bleach [15,16]. It is also an indispensable potent disinfectant of the human immune system and a metabolite of aerobic organisms [17,18]. Nevertheless, the excessive use of ClO$^-$ seriously threatens human health, resulting in various diseases and disorders, such as immunodeficiency, neurasthenia, atherosclerosis, nephropathy, and cancer [19–26]. Therefore, it is important to effectively monitor the ClO$^-$ content in the environment and organisms. Kateshiya et al. [11] synthesized carbon dots from the fruits of *Annona squamosa* and utilized them for the high-sensitivity

detection of ClO⁻ with a limit of detection (LOD) of 6.8 nmol·L^{-1}. Hu et al. [20] reported a ratiometric carbon dot with the advantages of high selectivity and rapid response for monitoring the ClO⁻ level. Wang et al. [27] reported boron-nitrogen-doped carbon nanodots for the detection of ClO⁻ in living cells and tap water. Duan et al. [28] synthesized a high-brightness red fluorescent probe for sensing HClO/ClO⁻ *in vitro* and *in vivo*. However, most of these materials present a few drawbacks, such as being environmentally unfriendly or causing waste of food resources.

Lignin is the most abundant renewable natural polymer material on earth, with an aromatic structure and a high carbon content [29]. The alkali lignin by-product produced by the pulp and paper industry amounts to tens of millions of tons annually [30]. However, the current utilization of lignin is extremely low, and most of it is treated as waste and directly discharged into rivers or burned, adversely affecting the environment. Hence, the efficient use of lignin and improvement of its added value have become a popular and urgent research topic. As an abundant and accessible carbon source, lignin has been actively developed as a fluorescent carbon-dot material in recent years. For instance, Ding et al. [31] synthesized lignin-based graphene quantum dots with blue fluorescence, which exhibited promising applications in the field of cell imaging. Jiang et al. [32] reported lignin-based blue carbon dots as fluorescent probes for the detection of Fe^{3+} ions. Zhang et al. [33] prepared lignin-based green fluorescent carbon dots that can be used in the fields of cell imaging and electrocatalysis.

In this work, new alkali lignin-derived carbon dots (SPN-CDs) with red fluorescence were synthesized based on the large sp^2 hybrid domain of lignin and the introduction of amino functional groups. Compared with the widely studied green and blue fluorescent carbon dots, which are more susceptible to short-wave background interfere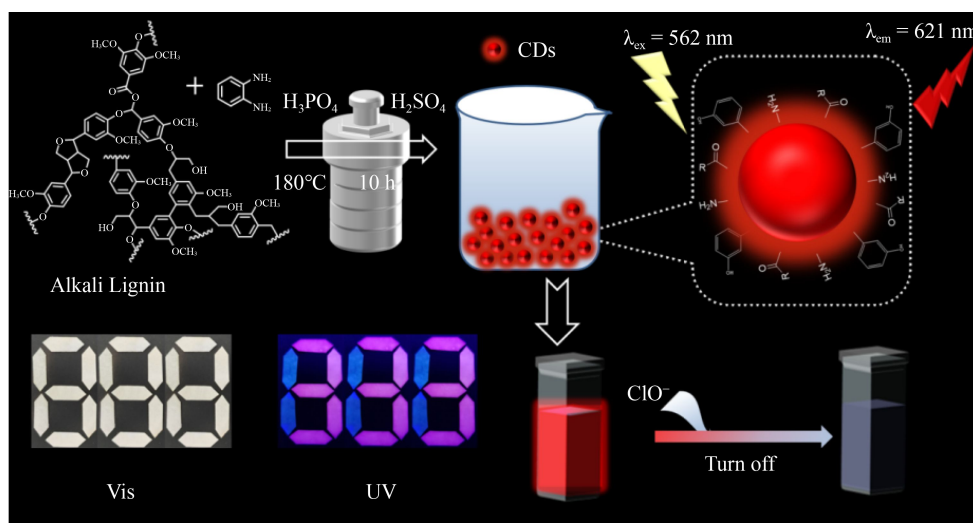nce, red carbon dots exhibit superior luminescence stability and penetrating power, allowing their application as stimuli-responsive fluorescent materials [34–39]. The prepared SPN-CDs exhibited a highly sensitive and selective optical response to ClO⁻ owing to the oxidation of hydroxybenzene to quinone, resulting in prominent changes in both visible color and fluorescence intensity. In this study, a portable, low-cost, and high-performance sensing paper based on SPN-CDs was fabricated, and its timely and sensitive detection of ClO⁻ was investigated.

Additionally, a new type of visible-light and fluorescent-dual-channel information encryption platform was constructed based on this promising SPN-CDs material, realizing diversified transmission or interference of information. Low concentrations of ClO⁻ can be employed as safe, accessible, and efficient information encryption/decryption stimuli. Interestingly, ClO⁻ can also function as an information "eraser" to destroy encrypted information after reading, significantly improving information security. This interesting feature is attributed to the different optical characteristic structural changes of SPN-CDs upon treatment with ClO⁻ at different concentrations. The dual-function SPN-CDs material reported in this study shows great potential for applications in the fields of security monitoring, environmental protection, information encryption, anti-counterfeiting, and national security. This opens new avenues for the high-value-added application of lignin-based green fluorescent materials.

2 Experimental

2.1 Synthesis of SPN-CDs

SPN-CDs was synthesized by a one-pot hydrothermal process (Scheme 1). First, 5 mL phosphoric acid and

Scheme 1 The preparation of SPN-CDs and their application in ClO⁻ detection and anti-counterfeiting.

5 mL 40% sulfuric acid were respectively taken into 50 mL beaker, and then 0.1 g alkali lignin and 0.3 g *o*-phenylenediamine were dissolved in the mixed solution of phosphoric acid and sulfuric acid. Next, ultrasonic treatment was conducted until all dissolved, and then the solution was moved to Teflon-lined autoclave and heat treated at 180 °C for 10 h. The solution was then cooled to room temperature and dialyzed for 72 h with ultrapure water through a dialysis bag (MD77-10000). Finally, the solution outside the bag was concentrated with a rotary evaporator to obtain SPN-CDs.

2.2   Detection of ClO⁻

SPN-CDs solution was prepared from ultrapure water. Then, 3 μL ClO⁻ was gradually added to 3 mL SPN-CDs solution. The final concentration range of ClO⁻ is 0–0.5 mmol·L^{-1}. The mixture was left for 5 min at room temperature and the fluorescence spectra were recorded.

3   Results and discussion

3.1   Structural characterization of SPN-CDs

To further understand the chemical composition of SPN-CDs, transmission electron microscopy (TEM), Fourier-transform infrared (FTIR) spectroscopy, proton nuclear magnetic resonance (^{1}H NMR), and X-ray photoelectron spectroscopy (XPS) were performed (Fig. 1). As shown in Fig. 1(a), the TEM image shows that SPN-CDs have an uniform particle size distribution in the range of 1.5–6.0 nm, an average particle size of 4.561 nm, and a quasi-spherical shape. The well-resolved crystal lattice spacing of 0.194 nm was attributed to the (100) lattice of graphitic carbon. Furthermore, FTIR spectroscopy was used to investigate the surface groups of the SPN-CDs (Fig. 1(b)). The absorption peaks at 1508 and 2936 cm^{-1} can be attributed to aromatic C=C and C–H stretching vibrations. These results suggest that the SPN-CDs comprise aromatic backbones. Meanwhile, the characteristic peak of lignin at 3400 cm^{-1} corresponds to the stretching vibration of –OH, whereas the peaks at 1639 and 1127 cm^{-1} correspond to C=O and C–O vibrations, respectively. These results indicate that the SPN-CDs did not destroy the inherent structure of the lignin. In addition, a new C–N peak appeared at 1236 cm^{-1} in the FTIR spectrum of the SPN-CDs, which may have been caused by hydrothermal alkali activation [34]. Furthermore, the peaks found in the range of 6.80–7.80 ppm in the ^{1}H NMR spectrum of the SPN-CDs (Fig. 1(c)) can be attributed to the benzene ring, which is consistent with the FTIR results. The elemental composition of the SPN-CDs was investigated by XPS. As shown in Fig. 1(d), four peaks were observed at 284.42, 400.8, 531.37, and

134.1 eV, corresponding to the binding energies of C 1s, N 1s, O 1s, and P 2p, respectively. The splitting of the C 1s peak in the high-resolution XPS spectrum (Fig. 1(e)) revealed two peaks at 284.28 and 285.60 eV, correlated with C–C and C–N, respectively. In the high-resolution N 1s spectrum, two new peaks at 399.9 and 400.8 eV were assigned to C=N and C–N, respectively (Fig. S1, cf. Electronic Supplementary Material, ESM). Meanwhile, in the high-resolution O 1s spectrum, the peaks corresponding to C=O and C–O are observed at 530.7 and 532.20 eV, respectively (Fig. 1(f)). Moreover, in the high-resolution P 2p spectrum, the peaks associated with P–O and P–C/P–N are observed at 133.68 and 134.53 eV, respectively (Fig. S2, cf. ESM). The XPS results obtained correlate well with the FTIR and ^{1}H NMR results.

3.2   Optical properties of SPN-CDs

The optical properties of the SPN-CDs were determined by ultraviolet–visible (UV–Vis) and fluorescence spectroscopy (Fig. 2). As shown in Figs. 2(a) and S3 (cf. ESM), there are three broad absorption peaks at 230, 277, and 474 nm, which are associated with $\pi \rightarrow \pi^*$ or n $\rightarrow \pi^*$ electronic transitions in the aromatic sp^2 domain (C=C) and aromatic heterocyclic rings (C=N and C=O) [40]. Compared with lignin, the UV–Vis spectrum of the SPN-CDs exhibits a new absorption peak at 474 nm. This indicates that the electronic energy level transition was caused by the introduction of nitrogen atoms in the SPN-CDs. The excitation (at 562 nm) and emission (at 621 nm) spectra of the SPN-CDs are shown in Fig. 2(b). The large Stokes shift (59 nm) of the SPN-CDs prevents interference from the excitation spectrum. Interestingly, the emission of the SPN-CDs in the range of 310–580 nm red-shifted (Fig. 2(c)), and the luminescence intensity gradually decreased with increasing excitation wavelength. This excitation-related property was attributed to the surface defects mainly generated by surface oxidation. These defects can trap excitons, resulting in a different energy gap and red shifting the emission wavelength of the SPN-CDs. The electronic transitions of the carbon nucleus in the range of 210–300 nm are mainly $\pi \rightarrow \pi^*$ transitions. Because the surface defects of the SPN-CDs make it difficult to capture the excited electrons of the carbon nucleus, there is no red-shift phenomenon observed in the excitation wavelength below 300 nm. Meanwhile, it can be observed from the chromaticity diagram (Fig. 2(d)) that the emission color of the carbon dots is red. Moreover, the fluorescence intensity and emission wavelength of the SPN-CDs did not change significantly under continuous UV irradiation for 2.5 h. This indicates the stability of the SPN-CDs under continuous UV irradiation (Fig. S4, cf. ESM). Furthermore, the fluorescence intensity and emission wavelength of the SPN-CDs did not show any noticeable changes with an increase in the concentration of NaCl (Fig. S5, cf.
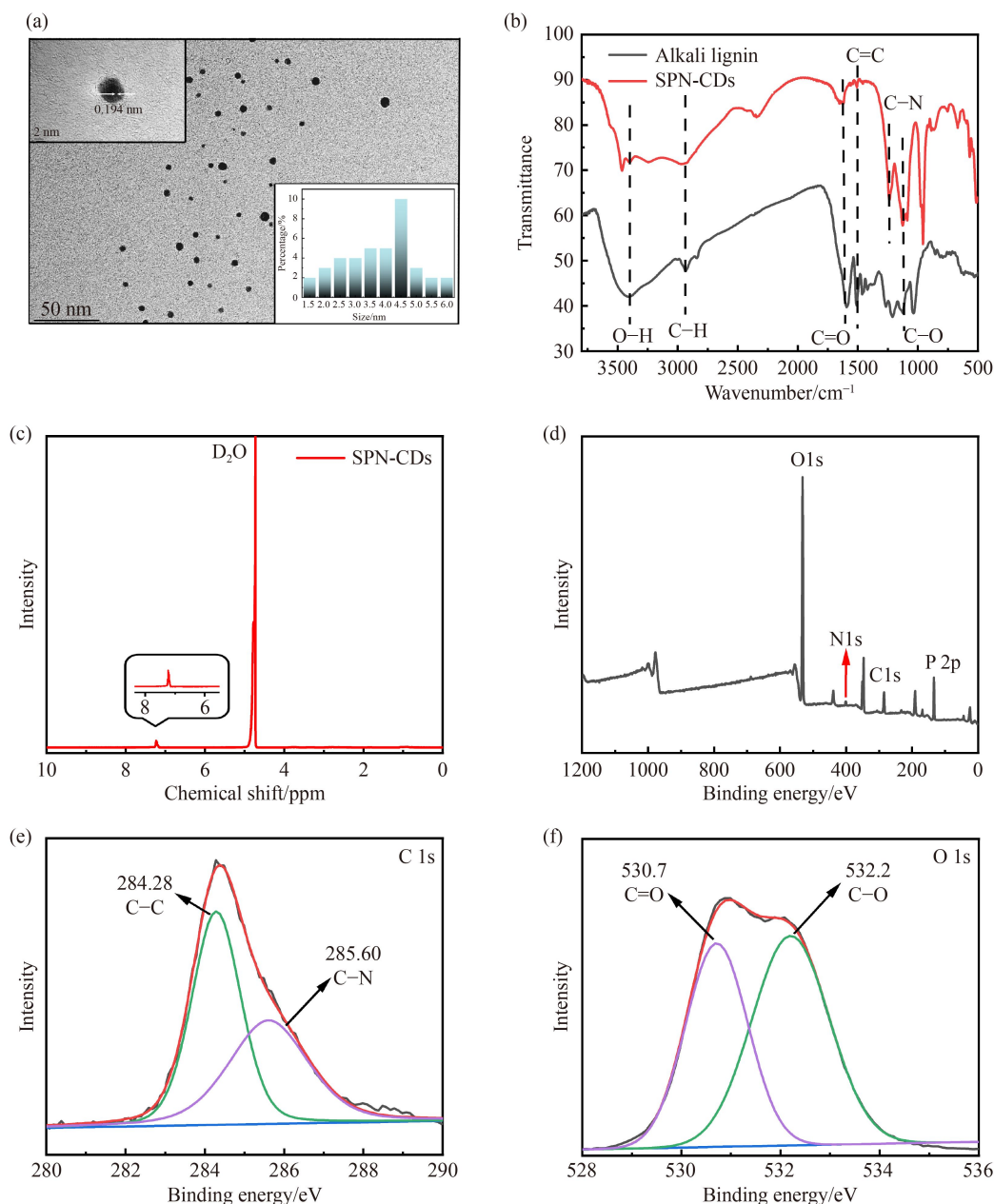
Fig. 1   (a) TEM images of SPN-CDs particles; (b) FTIR spectra of alkali lignin and SPN-CDs; (c) ^{1}H NMR spectrum of SPN-CDs in D_2O; (d–f) XPS spectrum and high-resolution XPS spectra of SPN-CDs.

ESM). Based on these results, the SPN-CDs can be used for detecting ClO$^-$ in complex environments with potential practical applications.

3.3   Sensing performance

The sensing performance of the SPN-CDs for various ClO$^-$ was evaluated using an RF-6000 fluorescence spectrometer (Fig. 3). As shown in Fig. 3(a), the fluorescence intensity of the SPN-CDs gradually decreased after exposure to ClO$^-$ and reached 90% quenching in approximately 17 s. The quenching efficiency as a function of the concentration of ClO$^-$ shows good

linearity in the range of 0–0.5 mmol·L^{-1} (Fig. 3(b)). Furthermore, the SPN-CDs exhibited a high sensitivity to ClO$^-$, and the LOD was calculated to be 0.249 μmol·L^{-1} (Fig. 3(c)), which is an excellent result (Table S1, cf. ESM). The influence of metal cations (Cu^{2+}, Co^{2+}, Ni^{2+}, Mg^{2+}, Pb^{2+}, Fe^{2+}, Mn^{2+}, Al^{3+}, K$^+$, Hg^{2+}, and Na$^+$), interfering anions (ClO$_4^-$, NO$_2^-$, NO$_3^-$, and I$^-$), and radical species on the fluorescence intensity of the SPN-CDs was also investigated (Figs. 3(d) and S6, cf. ESM). The SPN-CDs exhibited high selectivity for ClO$^-$, indicated by a prominent color change, and the fluorescence response of the SPN-CDs to these representative analytes was negligible.
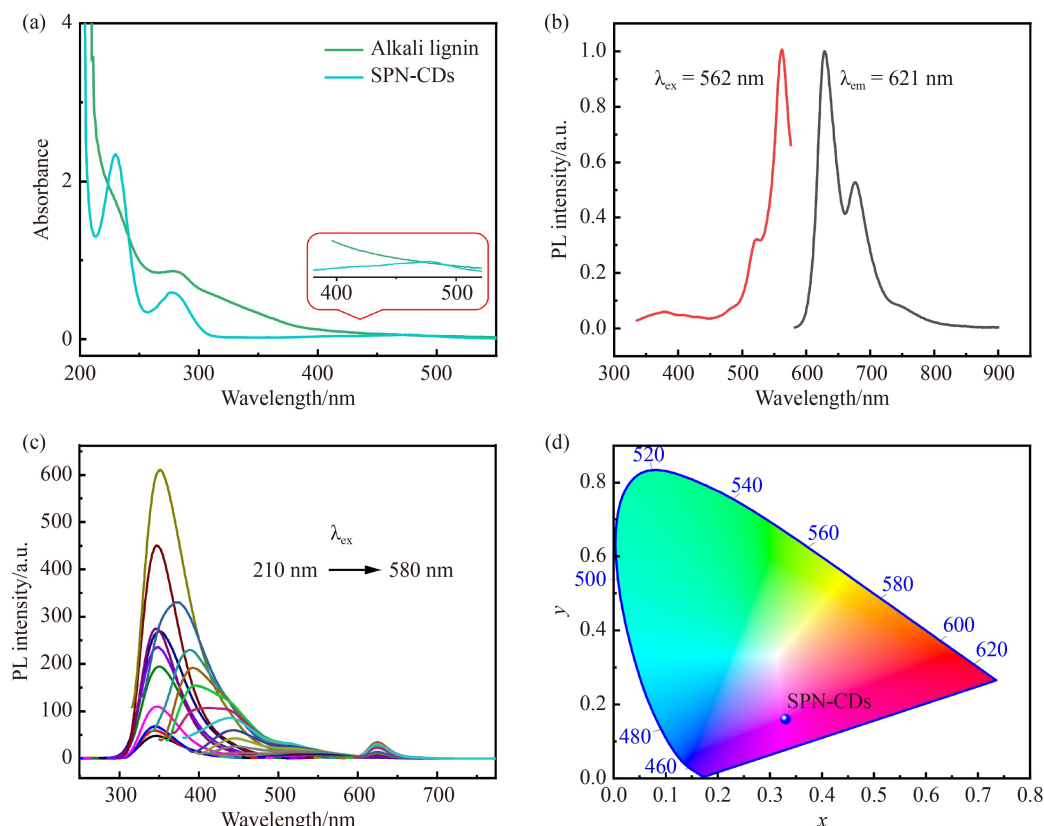
Fig. 2 (a) Absorption spectra of alkali lignin and SPN-CDs; (b) excitation and emission spectra of SPN-CDs; (c) fluorescence spectrum of the SPN-CDs at different excitation wavelengths from 210 to 580 nm; (d) the position of SPN-CDs corresponds to the chromaticity diagram 1931 XYZ color.

3.4   Quenching mechanism

The quenching mechanism of the SPN-CDs probe toward ClO^- was examined by UV–Vis spectroscopy, ^1H NMR, FTIR, and XPS (Fig. 4). As shown in Fig. 4(a), the UV–Vis characteristic peaks of the SPN-CDs at 450 nm increase significantly with the addition of low concentrations of ClO^- (0.2 mmol·L^{-1}), resulting in a color change from colorless to dark brown under visible light (the insert of Fig. 4(a)). This is due to the oxidation of the phenolic groups to quinone groups (Fig. S7, cf. ESM). Furthermore, with the addition of high concentrations of ClO^- (0.5 mmol·L^{-1}), the characteristic peak of the SPN-CDs at 450 nm began to decrease until it completely disappeared. This results in a color change from dark brown to colorless under visible light owing to further oxidation of the quinone group. In the FTIR spectrum of the SPN-CDs + ClO^- system (Fig. 4(b)), the peak at 1160 cm^{-1} was significantly reduced. This indicates that the phenolic group was oxidized, causing a change in the color of the solution (the insert of Fig. 4(a)). As shown in Fig. 4(c), the ^1H NMR peaks at 6.80–7.80 ppm disappeared owing to the change in the benzene ring structure due to the formation of quinone groups [41]. In addition, the XPS spectrum showed that the O and Cl contents in SPN-CDs + ClO^- substantially increased with

the addition of ClO^-, indicating that the C=O bond content increased significantly (Figs. S8–S13, cf. ESM). These results indicate that the oxidation of hydroxybenzene in SPN-CDs to quinone groups results in changes in both color and fluorescence intensity [27,42]. At high concentrations of hypochlorous acid, the skeletal structure of the chromophore was destroyed, causing the color to change to colorless (Fig. S14, cf. ESM). Furthermore, the fluorescence lifetimes of the SPN-CDs before and after the addition of ClO^- were determined (Fig. 4(d)). Compared to pure SPN-CDs (2.377 ns), the lifetimes of the SPN-CDs after the addition of ClO^- did not change significantly (2.407 ns), suggesting that the quenching mechanism follows a simple static quenching mechanism [43].

3.5   Preparation of solid sensors

For convenient and efficient on-site detection of ClO^-, preparing portable sensors is necessary (Fig. 5). Therefore, we doped the SPN-CDs into filter papers so that they were uniformly dispersed on the surface and inside the solid papers to obtain a solid sensor. The SPN-CDs-doped paper (Lanterns and Chinese knots) exhibited bright red fluorescence before exposure to ClO^-, whereas after exposure to ClO^-, the red fluorescence was rapidly
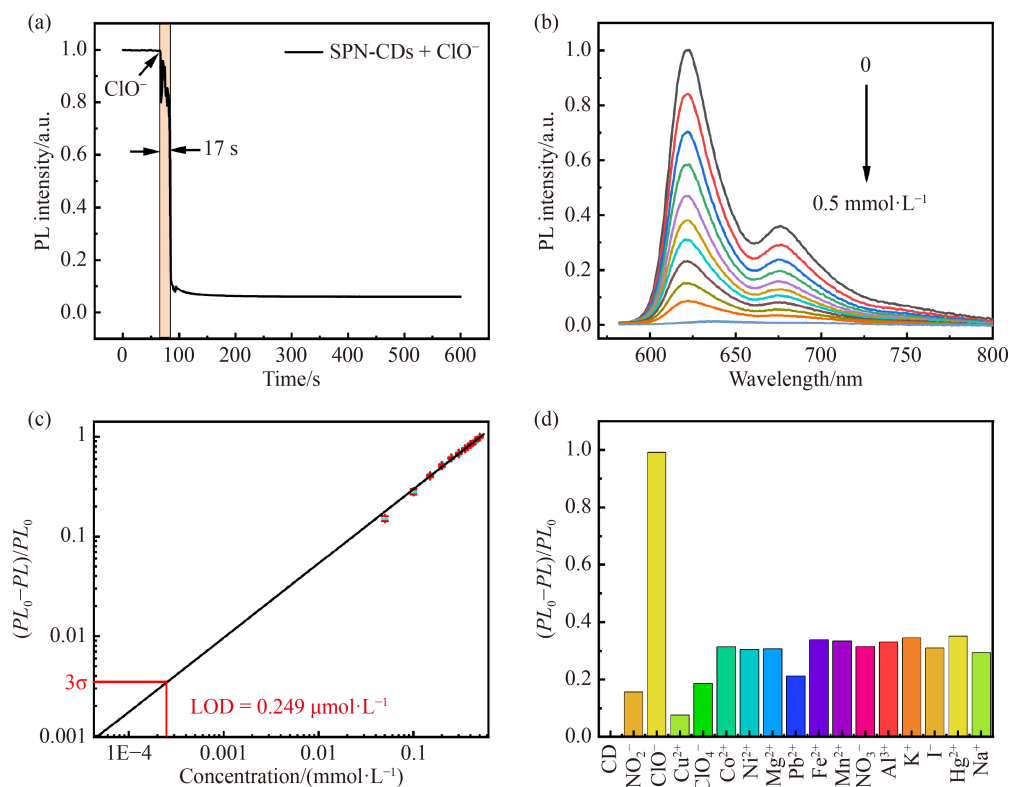
Fig. 3 (a) Time-dependent response of probe SPN-CDs to ClO^- (0.5 mmol·L^{-1}); (b) fluorescence response of SPN-CDs to various concentrations of ClO^- (0–0.5 mmol·L^{-1}) and (c) the corresponding linear relationship; (d) photoluminescence intensities change of the SPN-CDs probe to different kinds of metal cations and interfering anions (0.5 mmol·L^{-1}). λ_{ex} = 562 nm.
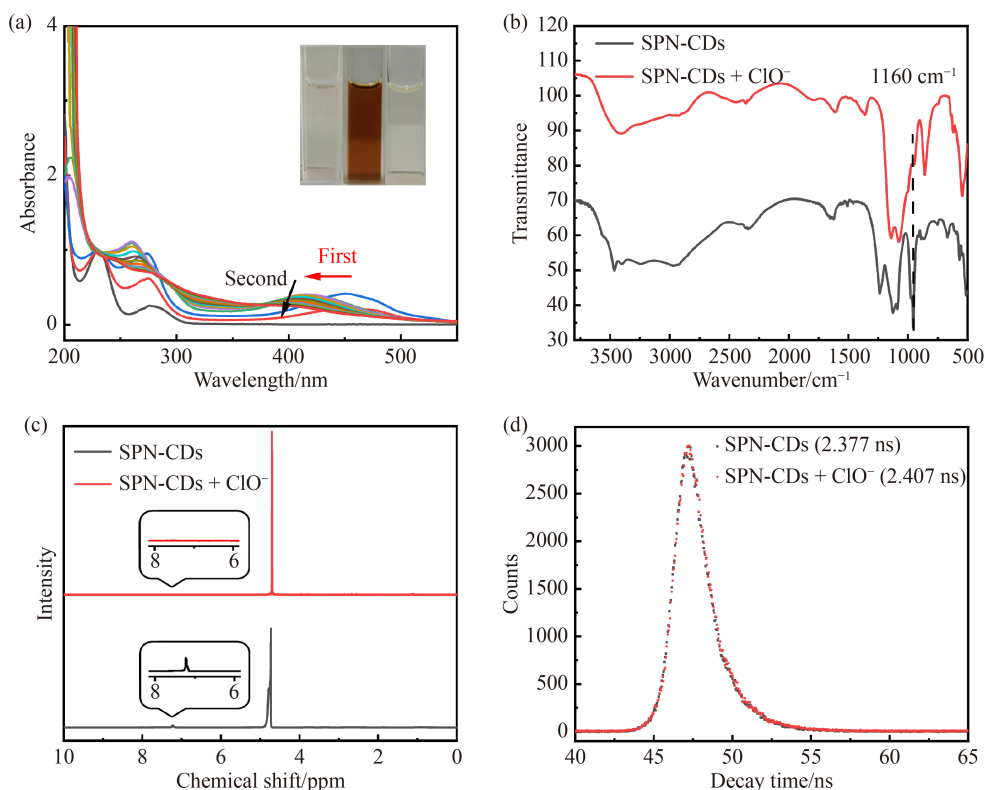

Fig. 4 (a) Absorption spectra of SPN-CDs with the addition of ClO^-; (b) FTIR spectrum of the SPN-CDs in the presence and absence of ClO^-; (c) ^{1}H NMR spectrum of SPN-CDs in the presence and absence of ClO^-; (d) fluorescence decays spectrum of the SPN-CDs in the presence and absence of ClO^-.

quenched and became colorless; this indicates that the SPN-CDs-doped paper could be used to detect ClO⁻ (Fig. 5(a)). As shown in Fig. 5(b), the fluorescence intensity of the SPN-CDs-doped paper gradually decreases with the gradual addition of ClO⁻ from 0 to 100 $\mu mol·L^{-1}$. Notably, the SPN-CDs-doped paper did not respond to other ions and exhibited a high selectivity for ClO⁻ (Fig. 5(c)). These solid-phase sensors provide an easy-to-prepare, low-cost, and pollution-free device to detect ClO⁻ in real environments.

3.6 Applications of encryption, decryption and anti-counterfeiting

For encryption and decryption anti-counterfeiting (Fig. 6), we applied low concentrations of the SPN-CDs (3 $mg·mL^{-1}$) for the preparation of the encrypted filter papers, and then some filter papers were treated with a high concentration of ClO⁻ (0.5 $mmol·L^{-1}$) for decryption. As shown in Fig. 6(a), the numeral "888" can be observed under visible-light irradiation, whereas under

UV light, the numeral "302" emits red fluorescence and the fluorescence of numeral "111" is quenched. This is attributed to the fact that the fluorescence of the SPN-CDs is quenched by ClO⁻, while the untreated carbon dots still exhibit red fluorescence, thus realizing monochromatic anti-counterfeiting of information. Moreover, we smeared a low concentration of carbon dots (10 $mg·mL^{-1}$) in the shape of a butterfly on a filter paper. As shown in Fig. 6(b), no information was observed under visible light, thus realizing information encryption. Under UV-light irradiation, the pattern was observed as red fluorescence, realizing the decryption of information. The filter paper with the butterfly pattern was then treated with a low concentration of ClO⁻ (25 $\mu mol·L^{-1}$), and the pattern could be observed under visible light. However, no information could be observed under UV light. Finally, when the filter paper was treated with a high concentration of ClO⁻ (50 $\mu mol·L^{-1}$), no information was observed under either visible or UV light.

Therefore, a dual-channel information encryption platform was successfully fabricated to realize the diversified transmission or interference of information. We wrote on a filter paper using a low-concentration SPN-CDs (3 $mg·mL^{-1}$) pen. The words became colorless under visible light and exhibited red fluorescence under ultraviolet light (Fig. 7). The filter paper was then smeared with a low concentration of ClO⁻ (0.2 $mmol·L^{-1}$), and the smear was visible under visible light. Simultaneously, information on the smeared part was permanently erased by smearing again directly with a high concentration of ClO⁻ (0.5 $mmol·L^{-1}$). In addition, the words smeared with ClO⁻ were permanently erased under UV light. We then used carbon dots as ink to write the words again on the filter paper, which can be read under visible light but no words were observed under ultraviolet light. Thus, the encryption, double decryption, and elimination of information were achieved (Video S1, cf. ESM).
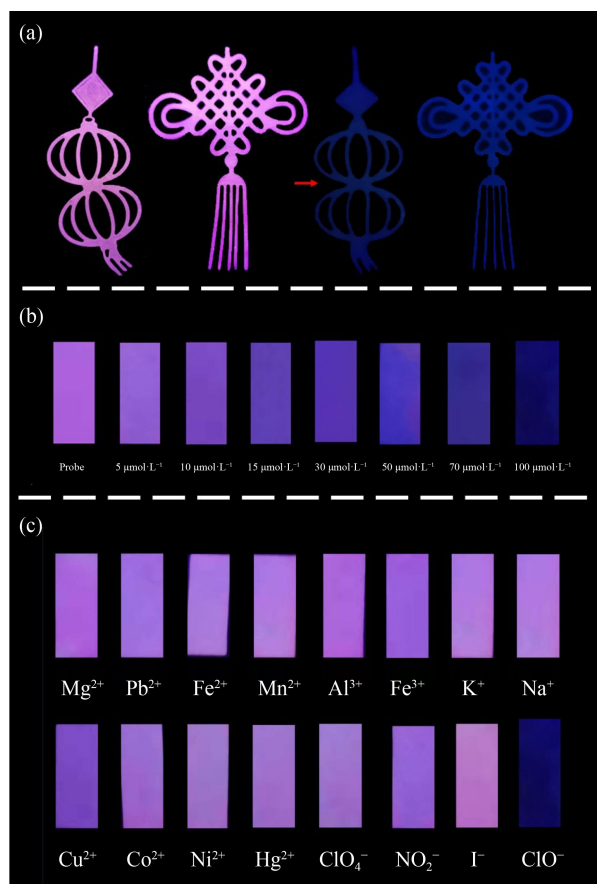

Fig. 5 (a) Photographs of SPN-CDs-doped paper before (left) and after (right) the addition of ClO⁻ under the irradiation of UV light; (b) photographs of the quantitative card of SPN-CDs-doped paper for ClO⁻ detection; (c) the selective test of SPN-CDs-doped paper for ClO⁻ detection.
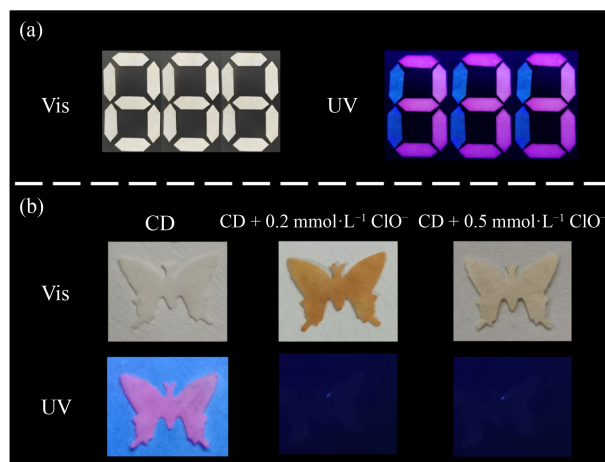

Fig. 6 (a) Digital anti-counterfeiting; (b) SPN-CDs are used for encryption and double decryption of information.
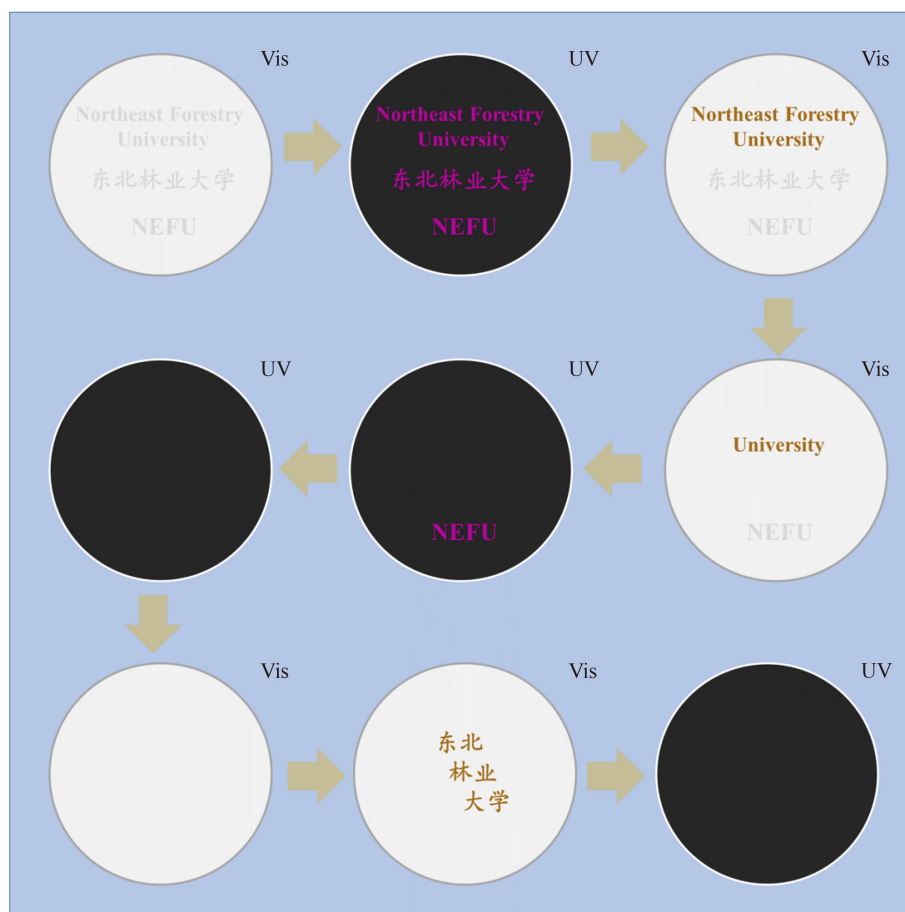
Fig. 7   Schematic diagram of SPN-CDs are used for encryption and decryption of information.

4   Conclusions

In brief, we prepared red fluorescence SPN-CDs based on lignin, which exhibited good water solubility, strong fluorescence intensity, and abundant surface functional groups, by a hydrothermal reaction. The SPN-CDs exhibited good linear recognition performance for ClO⁻ aqueous solutions and excellent sensitivity. In addition, SPN-CDs-doped papers can be used as low-cost and simple solid fluorescence sensors for the rapid detection of ClO⁻. Notably, the SPN-CDs-doped paper can realize a high level of encryption, decryption, and anti-counterfeiting properties under the stimulation of different concentrations of ClO⁻.

References

1. Espina-Casado J, Fernández-González A, Díaz-García M E, Badía-Laíño R. Smart carbon dots as chemosensor for control of water contamination in organic media. Sensors and Actuators B: Chemical, 2021, 329: 129262

2. Ahmed F, Iqbal S, Zhao L, Xiong H. "On-off-on" fluorescence switches based on N,S-doped carbon dots: facile hydrothermal growth, selective detection of Hg²⁺, and as a reversive probe for guanine. Analytica Chimica Acta, 2021, 1183: 338977

3. Li L, Ren X, Bai P, Liu Y, Xu W, Xie J, Zhang R. Near-infrared emission carbon dots for bio-imaging applications. New Carbon Materials, 2021, 36(3): 632–638

4. Wan J, Zhang X, Fu K, Zhang X, Shang L, Su Z. Highly fluorescent carbon dots as novel theranostic agents for biomedical applications. Nanoscale, 2021, 13(41): 17236–17253

5. Xie A Q, Guo J, Zhu L, Chen S. Carbon dots promoted photonic crystal for optical information storage and sensing. Chemical Engineering Journal, 2021, 415: 128950

6. Muthamma K, Sunil D, Shetty P. Carbon dots as emerging luminophores in security inks for anti-counterfeit

applications—an up-to-date review. Applied Materials Today, 2021, 23: 101050

7. Zhang J, He B, Hu Y, Alam P, Zhang H, Lam J W Y, Tang B Z. Stimuli-responsive AIEgens. Advanced Materials, 2021, 33(32): 2008071

8. Zhou H, Han J, Cuan J, Zhou Y. Responsive luminescent MOF materials for advanced anticounterfeiting. Chemical Engineering Journal, 2022, 431: 134170

9. Liu H, Wang Y, Mo W, Tang H, Cheng Z, Chen Y, Zhang S, Ma H, Li B, Li X. Dendrimer-based, high-luminescence conjugated microporous polymer films for highly sensitive and selective volatile organic compound sensor arrays. Advanced Functional Materials, 2020, 30(13): 1910275

10. Li X, Zhao S, Li B, Yang K, Lan M, Zeng L. Advances and perspectives in carbon dot-based fluorescent probes: mechanism, and application. Coordination Chemistry Reviews, 2021, 431: 213686

11. Kateshiya M R, Malek N I, Kumar Kailasa S. Green fluorescent carbon dots functionalized MoO_3 nanoparticles for sensing of hypochlorite. Journal of Molecular Liquids, 2022, 351: 118628

12. Kailasa S K, Koduru J R. Perspectives of magnetic nature carbon dots in analytical chemistry: from separation to detection and bioimaging. Trends in Environmental Analytical Chemistry, 2022, 33: e00153

13. Ashrafizadeh M, Mohammadinejad R, Kailasa S K, Ahmadi Z, Afshar E G, Pardakhty A. Carbon dots as versatile nanoarchitectures for the treatment of neurological disorders and their theranostic applications: a review. Advances in Colloid and Interface Science, 2020, 278: 102123

14. Yu H, Shi R, Zhao Y, Waterhouse G I N, Wu L Z, Tung C H, Zhang T. Smart utilization of carbon dots in semiconductor photocatalysis. Advanced Materials, 2016, 28(43): 9454–9477

15. Wilhelm N, Kaufmann A, Blanton E, Lantagne D. Sodium hypochlorite dosage for household and emergency water treatment: updated recommendations. Journal of Water and Health, 2017, 16(1): 112–125

16. Wu H, Zhang W, Wu Y, Liu N, Meng F, Xie Y, Yan L A. 7-Diethylaminocoumarin-based chemosensor with barbituric acid for hypochlorite and hydrazine. Microchemical Journal, 2020, 159: 105461

17. Yang G, Wan X, Su Y, Zeng X, Tang J. Acidophilic S-doped carbon quantum dots derived from cellulose fibers and their fluorescence sensing performance for metal ions in an extremely strong acid environment. Journal of Materials Chemistry A: Materials for Energy and Sustainability, 2016, 4(33): 12841–12849

18. Wang Z, Zhang Y, Song J, Li M, Yang Y, Gu W, Xu X, Xu H, Wang S. A highly specific and sensitive turn-on fluorescence probe for hypochlorite detection based on anthracene fluorophore and its bioimaging applications. Dyes and Pigments, 2019, 161: 172–181

19. Ji D, Li G, Zhang S, Zhu M, Li C, Qiao R. Mitochondria-targeted fluorescence probe for endogenous hypochlorite imaging in living cells and zebrafishs. Sensors and Actuators B: Chemical, 2018, 259: 816–824

20. Hu Q, Qin C, Huang L, Wang H, Liu Q, Zeng L. Selective

visualization of hypochlorite and its fluctuation in cancer cells by a mitochondria-targeting ratiometric fluorescent probe. Dyes and Pigments, 2018, 149: 253–260

21. Tang C, Gao Y, Liu T, Lin Y, Zhang X, Zhang C, Li X, Zhang T, Du L, Li M. Bioluminescent probe for detecting endogenous hypochlorite in living mice. Organic & Biomolecular Chemistry, 2018, 16(4): 645–651

22. Zhu B, Wu L, Zhang M, Wang Y, Liu C, Wang Z, Duan Q, Jia P. A highly specific and ultrasensitive near-infrared fluorescent probe for imaging basal hypochlorite in the mitochondria of living cells. Biosensors & Bioelectronics, 2018, 107: 218–223

23. Xi L L, Guo X F, Wang C L, Wu W L, Huang M F, Miao J Y, Zhao B X. A near-infrared ratiometric fluorescent probe for rapid and selective detection of hypochlorous acid in aqueous solution and living cells. Sensors and Actuators B: Chemical, 2018, 255: 666–671

24. Yue Y, Huo F, Yin C, Escobedo J O, Strongin R M. An recent progress in chromogenic and fluorogenic chemosensors for hypochlorous acid. Analyst, 2016, 141(6): 1859–1873

25. Chen X, Wang F, Hyun J Y, Wei T, Qiang J, Ren X, Shin I, Yoon J. Recent progress in the development of fluorescent, luminescent and colorimetric probes for detection of reactive oxygen and nitrogen species. Chemical Society Reviews, 2016, 45(10): 2976–3016

26. Feng Y, Li S, Li D, Wang Q, Ning P, Chen M, Tian X, Wang X. Rational design of a diaminomaleonitrile-based mitochondria-targeted two-photon fluorescent probe for hypochlorite *in vivo*: solvent-independent and high selectivity over Cu^{2+}. Sensors and Actuators B: Chemical, 2018, 254: 282–290

27. Wang Z X, Jin X, Gao Y F, Kong F Y, Wang W J, Wang W. Fluorometric and colorimetric determination of hypochlorite using carbon nanodots doped with boron and nitrogen. Mikrochimica Acta, 2019, 186(6): 328

28. Duan C, Won M, Verwilst P, Xu J, Kim H S, Zeng L, Kim J S. *In vivo* imaging of endogenously produced HClO in zebrafish and mice using a bright, photostable ratiometric fluorescent probe. Analytical Chemistry, 2019, 91(6): 4172–4178

29. Hu H C, Xu H, Wu J, Li L, Yue F, Huang L, Chen L, Zhang X, Ouyang X. Secondary bonds modifying conjugate-blocked linkages of biomass-derived lignin to form electron transfer 3D networks for efficiency exceeding 16% nonfullerene organic solar cells. Advanced Functional Materials, 2020, 30(23): 2001494

30. Agarwal A, Rana M, Park J H. Advancement in technologies for the depolymerization of lignin. Fuel Processing Technology, 2018, 181: 115–132

31. Ding Z, Li F, Wen J, Wang X, Sun R. Gram-scale synthesis of single-crystalline graphene quantum dots derived from lignin biomass. Green Chemistry, 2018, 20(6): 1383–1390

32. Jiang X, Shi Y, Liu X, Wang M, Song P, Xu F, Zhang X. Synthesis of nitrogen-doped lignin/DES carbon quantum dots as a fluorescent probe for the detection of Fe^{3+} ions. Polymers, 2018, 10(11): 1282

33. Zhang B, Liu Y, Ren M, Li W, Zhang X, Vajtai R, Ajayan P M, Tour J M, Wang L. Sustainable synthesis of bright green fluorescent nitrogen-doped carbon quantum dots from alkali lignin. ChemSusChem, 2019, 12(18): 4202–4210

34. Zhu X, Yuan X, Han L, Liu H, Sun B. A smartphone-integrated optosensing platform based on red-emission carbon dots for real-time detection of pyrethroids. Biosensors & Bioelectronics, 2021, 191: 113460

35. Wang X, Cheng Z, Zhou Y, Tammina S K, Yang Y. A double carbon dot system composed of N, Cl-doped carbon dots and N, Cu-doped carbon dots as peroxidase mimics and as fluorescent probes for the determination of hydroquinone by fluorescence. Mikrochimica Acta, 2020, 187(6): 350

36. Fan Y Z, Tang Q, Liu S G, Yang Y Z, Ju Y J, Xiao N, Luo H Q, Li N B. A smartphone-integrated dual-mode nanosensor based on novel green-fluorescent carbon quantum dots for rapid and highly selective detection of 2,4,6-trinitrophenol and pH. Applied Surface Science, 2019, 492: 550–557

37. Pathak A, Pv S, Stanley J, Satheesh Babu T G. Correction to: multicolor emitting N/S-doped carbon dots as a fluorescent probe for imaging pathogenic bacteria and human buccal epithelial cells. Mikrochimica Acta, 2019, 186(9): 645

38. Lu H, Xu S, Liu J. One pot generation of blue and red carbon dots in one binary solvent system for dual channel detection of Cr^{3+} and Pb^{2+} based on ion imprinted fluorescence polymers. ACS Sensors, 2019, 4(7): 1917–1924

39. Jia R, Jin K, Zhang J, Zheng X, Wang S, Zhang J. Colorimetric and fluorescent detection of glutathione over cysteine and homocysteine with red-emitting N-doped carbon dots. Sensors and Actuators B: Chemical, 2020, 321: 128506

40. Lu S, Sui L, Liu J, Zhu S, Chen A, Jin M, Yang B. Near-infrared photoluminescent polymer-carbon nanodots with two-photon fluorescence. Advanced Materials, 2017, 29(15): 1603443

41. Yang J, Jin X, Cheng Z, Zhou H, Gao L, Jiang D, Jie X, Ma Y, Chen W. Facile and green synthesis of bifunctional carbon dots for detection of Cu^{2+} and ClO^- in aqueous solution. ACS Sustainable Chemistry & Engineering, 2021, 9(39): 13206–13214

42. Zhang P, Wang Y, Chen L, Yin Y. Bimetallic nanoclusters with strong red fluorescence for sensitive detection of hypochlorite in tap water. Mikrochimica Acta, 2017, 184(10): 3781–3787

43. Wang Z X, Ding S N. One-pot green synthesis of high quantum yield oxygen-doped, nitrogen-rich, photoluminescent polymer carbon nanoribbons as an effective fluorescent sensing platform for sensitive and selective detection of silver(I) and mercury(II) ions. Analytical Chemistry, 2014, 86(15): 7436–7445